Robust Emergency Preparedness Planning for Resilience Enhancement of Energy-Transportation Nexus Against Extreme Rainfalls

Zhihao Hua, *Graduate Student Member, IEEE*, Bin Zhou, *Senior Member, IEEE*, Siu Wing Or, Jie Zhang, *Senior Member, IEEE*, Canbing Li, *Senior Member, IEEE*, and Juan Wei

***Abstract*—This article proposes a robust emergency preparedness planning (EPP) scheme to optimally pre-position diverse mobile emergency resources (MERs) in staging locations and perform proactive network reconfiguration for resilience enhancement of energy-transportation nexus (ETN) against extreme rainfalls. Based on rainfall-runoff simulation with hydrodynamic partial differential equations, a risk identification approach for flood-prone transportation modeling is developed for vehicle travel time estimation and MER routing optimization. To handle uncertainties in line outages and flooded roads incurred by extreme rainfalls, a tri-level robust EPP model is proposed to determine the optimal emergency preparedness plan immunized against the worst-case realization of uncertainties. Furthermore, a tailored solution method combining nested column-and-constraint generation algorithm with multiple linearization techniques is devised to cope with the proposed nonlinear robust EPP model. Comparative studies have validated the effectiveness of the proposed scheme for resilience enhancement of the ETN confronted with extreme rainfall disasters.**

Manuscript received 15 January 2023; revised 9 April 2023; accepted 30 April 2023. Date of publication 9 May 2023; date of current version 18 January 2024. Paper 2022-HTES-1556.R1, approved for publication in the IEEE TRANSACTIONS ON INDUSTRY APPLICATIONS by the Advances in Energy Conversion, Control, Operation and Planning Towards Self-Sustained of the IEEE Industry Applications Society. This work was supported in part by the Research Grants Council of the HKSAR Government under Grant R5020-18, in part by the Innovation and Technology Commission of the HKSAR Government to the Hong Kong Branch of National Rail Transit Electrification and Automation Engineering Technology Research Center under Grant K-BBY1, in part by the National Natural Science Foundation of China under Grants 52277091 and 51877072, and in part by the Hunan Natural Science Foundation of China under Grant 2021JJ10019. *(Corresponding authors: Bin Zhou; Juan Wei.)*

Zhihao Hua is with the College of Electrical and Information Engineering, Hunan University, Changsha 410082, China, also with the Department of Electrical Engineering, The Hong Kong Polytechnic University, Hong Kong SAR, China, and also with the Hong Kong Branch of National Rail Transit Electrification and Automation Engineering Technology Research Center, Hong Kong SAR, China (e-mail: hua_zhi_hao@hnu.edu.cn).

Bin Zhou and Juan Wei are with the College of Electrical and Information Engineering, Hunan University, Changsha 410082, China (e-mail: binzhou@hnu.edu.cn; weijuanba@hnu.edu.cn).

Siu Wing Or is with the Department of Electrical Engineering, The Hong Kong Polytechnic University, Hong Kong SAR, China, and also with the Hong Kong Branch of National Rail Transit Electrification and Automation Engineering Technology Research Center, Hong Kong SAR, China (e-mail: eeswor@polyu.edu.hk).

Jie Zhang is with the Department of Mechanical Engineering and (Affiliated) Department of Electrical and Computer Engineering, The University of Texas at Dallas, Richardson, TX 75080 USA (e-mail: jiezhang@utdallas.edu).

Canbing Li is with the Department of Electrical Engineering, Shanghai Jiao Tong University, Shanghai 200240, China (e-mail: licanbing@sjtu.edu.cn).

Color versions of one or more figures in this article are available at https://doi.org/10.1109/TIA.2023.3274615.

Digital Object Identifier 10.1109/TIA.2023.3274615

***Index Terms*—Energy-transportation nexus, disaster preparedness, mobile emergency resources, optimal proactive planning, extreme rainfall.**

NOMENCLATURE

Abbreviations

C&CG	Column-and-constraint generation.
DG	Distributed generator.
ETN	Energy-transportation nexus.
EDV	Emergency drainage vehicle.
EPP	Emergency preparedness planning.
MER	Mobile emergency resource.
MEG	Mobile emergency generator.
MESS	Mobile energy storage system.
MILP	Mixed-integer linear programming.
MPS	Mobile power source.
NC&CG	Nested column-and-constraint generation.
1D SVEs	One-dimensional Saint-Venant equations.
RCS	Remote-control switch.
2D SWEs	Two-dimensional shallow water equations.
WT	Wind turbine.

Sets

$\mathcal{T}/\mathcal{T}'$	Set of time periods in the upper/lower level.
$\mathcal{V}$	Set of all MPSs and EDVs.
$\mathcal{V}_{\rm P}/\mathcal{V}_{\rm D}/\mathcal{V}_{\rm G}/\mathcal{V}_{\rm S}$	Set of MPSs/EDVs/MEGs/MESSs, and $\mathcal{V}_{\rm P}/\mathcal{V}_{\rm D}/\mathcal{V}_{\rm G}/\mathcal{V}_{\rm S} \subseteq \mathcal{V}$.
$\mathcal{N}/\mathcal{G}$	Set of nodes/staging locations in the transportation network, and $\mathcal{G} \subseteq \mathcal{N}$.
$\mathcal{B}/\mathcal{L}$	Set of buses/lines, and $\mathcal{L} \subseteq \mathcal{B} \times \mathcal{B}$.
$\mathcal{R}/\mathcal{R}_{\rm f}/\mathcal{R}_{\rm fp}$	Set of real roads/fictitious roads/flood-prone roads, and $\mathcal{R}/\mathcal{R}_{\rm f}/\mathcal{R}_{\rm fp} \subseteq \mathcal{N} \times \mathcal{N}$.
$\mathcal{K}_{gj}$	Set of routes connecting node g and j.
$end(r)$	Set of ends of road r, and $end(r) \subseteq \mathcal{N}$.
$\mathcal{N}_{\rm f}$	Set of ends of flood-prone roads, and $\mathcal{N}_{\rm f} := \{i : i \in end(r)\ \forall r \in \mathcal{R}_{\rm fp}\} \subseteq \mathcal{N}$.
$\mathcal{N}_{\rm ac}$	Set of nodes at which MPSs can be connected to the distribution network.

Parameters

$C_{\langle j \rangle}$	Allowable total capacities of MPSs connected to bus $\langle j \rangle$.

0093-9994 © 2023 IEEE. Personal use is permitted, but republication/redistribution requires IEEE permission.
See https://www.ieee.org/publications/rights/index.html for more information.

Authorized licensed use limited to: Univ of Texas at Dallas. Downloaded on January 21,2024 at 03:38:14 UTC from IEEE Xplore. Restrictions apply.

$\bar{d}_i$ Upper limit of $d^j_{i,t}$.
$h_{r,t'}$ Inundation depth of road r at time t' obtained from the rainfall-runoff simulation.
K_g Allowable number of MPSs and EDVs pre-positioned in staging location g.
$\bar{P}^{\mathrm{G}}_i/\bar{P}^{\mathrm{S}}_i$ Maximum active power output of MEG/MESS i.
$P_{i,t}/Q_{i,t}$ Active/reactive demand at bus i and time t.
$\bar{P}^{\mathrm{wt}}_{i,t}$ Forecasted WT generation at bus i and time t.
P^{rp}_i Maximum ramping limit of DG at bus i.
r_{ij}/x_{ij} Resistance/reactance of line (i,j).
$\bar{S}_{ij}$, $\bar{S}^{\mathrm{dg}}_i$, $\bar{S}^{\mathrm{wt}}_i$ Rated apparent power capacities of line (i,j), DG at bus i, and WT at bus i.
$\tilde{T}_r$ Free travel time on road r.
$T^{\mathrm{v}_i g}_t$ Known travel time from initial location v_i to node g at time t.
T_{ER} Estimated time when extreme rainfall occurs.
T^{co}_i Time required for connecting MPS i to the distribution network.
ΔT Duration of each time period.
$\Delta T^{\mathrm{d}}_{ij}$ Repair time of line (i,j).
$\Phi_1,\Phi_2,\Psi_1,\Psi_2$ Uncertainty budgets.
$\delta^{gj}_{r,k}$ Binary parameter equals 1 if road r belongs to route $k \in \mathcal{K}_{gj}$.
$\eta^{\mathrm{Sd}}_b/\eta^{\mathrm{Sc}}_b$ Discharge/charge efficiency of MESS b.
$\underline{SoC}_b/\overline{SoC}_b$ Maximum/minimum SoC of MESS b.
v_i Initial location of vehicle i.
ω_i Priority weight of load at bus i.
ε/M A sufficiently small/large positive number.

Variables

$d^j_{i,t}$ Inundation depth decreased by EDV i at node j and time t'.
$H_{r,t'}$ Inundation depth of road r at time t' after drainage by EDVs.
$P^{\mathrm{in}}_{i,t}/Q^{\mathrm{in}}_{i,t}$ Active/reactive power injection at bus i and time t.
$P_{ij,t}/Q_{ij,t}$ Active/reactive power flow on line (i,j) at time t.
$P^{\mathrm{mg}}_{i,t}/Q^{\mathrm{mg}}_{i,t}$ Active/reactive power imported from the main grid.
$P^{\mathrm{dg}}_{i,t}/Q^{\mathrm{dg}}_{i,t}$ Active/reactive power output of DG at bus i and time t.
$P^{\mathrm{wt}}_{i,t}/Q^{\mathrm{wt}}_{i,t}$ Active/reactive power output of WT at bus i and time t.
$P^{\mathrm{G}}_{a,i,t'}/Q^{\mathrm{G}}_{a,i,t'}$ Active/reactive power output of MEG a at bus i and time t'.
$P^{\mathrm{S}}_{b,i,t'}$ Active power output of MESS b at bus i and time t'
$P^{\mathrm{Sd}}_{b,t'}/P^{\mathrm{Sc}}_{b,t'}$ Discharging/charging power of MESS b at time t'.
$\Delta P_{i,t'}/\Delta Q_{i,t'}$ Active/reactive load curtailment at bus i and time t'.
$T_{r,t'}$ Travel time on road r at time t'.
$T^{gj}_{k,t'}$ Travel time on route $k \in \mathcal{K}_{gj}$ at time t'.
$V_{i,t}$ Squared voltage magnitude of bus i at time t.
$\mu^{\mathrm{Sd}}_{b,t'}/\mu^{\mathrm{Sc}}_{b,t'}$ Binary variable indicates discharge/charge status of MESS b at time t'.
$SoC_{b,t'}$ SoC in MESS b at time t'.
$\alpha_{ij,t}$ Binary variable equals 1/0 if line (i,j) is closed/open at time t.
$\beta_{ij,t}$ Binary variable equals 1 if bus j is the parent of bus i at time t.
$\gamma^{\mathrm{v}_i g}_{i,t}$ Binary variable equals 1 if vehicle i travels from initial location v_i to node g at time t.
$\gamma^{gj}_{i,k,t'}$ Binary variable equals 1 if vehicle i travels from node g to j via route k at time t'.
δ_{ij} Binary variable equals 1 if line (i,j) is damaged during the extreme rainfall.
$\phi_{ij,t'}$ Binary variable equals 0 if line (i,j) is damaged at time t'.
ψ_r Binary variable equals 1 if road r is flooded during the extreme rainfall.
$z^j_{i,t'}$ Binary variable equals 1 if EDV i is at node j at time t'.
$\xi^j_{i,t'}$ Binary variable equals 1 if vehicle i arrives at node j at time t'.
$u^{\langle j\rangle}_{i,t'}$ Binary variable equals 1 if MPS i is connected to bus $\langle j\rangle$ at time t'.

I. Introduction

A. Motivation

DRIVEN by ongoing transportation electrification, energy-transportation nexus (ETN) has received burgeoning interest in recent years, since it offers a promising solution to increase the utilization of distributed renewable resources and accelerate the transition to a carbon-neutral highway transportation system [1]. However, interdependencies among infrastructure systems expose the ETN to compound disasters and cascading failures under extreme weather [2]. Among the most destructive weather disasters, extreme rainfalls have been observed to adversely affect the secure operations of energy systems with large-scale blackouts, and trigger widespread traffic disruptions to transportation systems with severe road flooding. Moreover, flooded roads threaten the nearby substations and distribution towers, and prevent mobile emergency resources (MERs) from responding, thereby exposing critical loads to power outage risks. Due to increasingly frequent and intense extreme rainfall events, the adverse impact of rainfall-induced destruction underscores the necessity of investigating effective resilience enhancement technologies for the ETN.

Pre-positioning of diverse MERs such as mobile power sources (MPSs) and emergency drainage vehicles (EDVs) can boost proactive emergency preparedness to effectively enhance the resilience of the ETN against extreme rainfalls [3], [4], [5]. The pre-positioned MPSs can be rapidly allocated in the ETN to help restore critical loads, and EDVs can mitigate road flooding to enable safe and time-saving travel of MPSs during service restoration. However, the lack of consideration of coordination between MPSs and EDVs unavoidably lead to

Authorized licensed use limited to: Univ of Texas at Dallas. Downloaded on January 21,2024 at 03:38:14 UTC from IEEE Xplore. Restrictions apply.

a biased pre-positioning plan that retards the recovery efforts. Furthermore, uncertain line outages and flooded roads, due to the uncertainty in the spatio-temporal distribution of precipitation intensity, further increase the complexity of developing a robust pre-positioning plan. Consequently, this article aims to investigate a robust emergency preparedness planning (EPP) scheme considering uncertainties in line outages and flooded roads to optimally pre-position MPSs and EDVs for resilience enhancement of the ETN against extreme rainfall disasters.

B. Literature Review

Various studies have investigated resilience enhancement technologies for energy-transportation systems against natural disasters, which mainly focused on infrastructure hardening [6], [7] and service restoration coordinated with the allocation of diverse MERs [8], [9], [10], [11], [12], [13], [14], [15]. The hardening of roads and power lines was studied in [6] and [7]. Generally, infrastructure hardening is a lengthy endeavor and entails substantial investment. The allocation of MERs, such as electric vehicles [8], [12] including electric buses [9] and E-taxis [11], repair crews [14], MPSs including mobile emergency generators (MEGs) and mobile energy storage systems (MESSs) [11], [12], [13], [14], [15], and mobile de-icing devices [10] has been comprehensively investigated to coordinate with network reconfiguration and microgrid formulation to help increase the restoration efficiency. Moreover, multiple transportation system models, such as the semi-dynamic traffic assignment model in [10], and route planning algorithms, such as Dijkstra's algorithm in [15], were adopted to minimize the travel time of MERs. These allocation efforts were conducted after the occurrence of disasters, which are not able to proactively boost the emergency preparedness of the ETN in the face of upcoming natural disasters. Proactive emergency preparedness offers significant advantages, notably in mitigating unintended negative impacts of natural disasters, improving post-disaster recovery efforts, and enhancing system resilience [3], [16]. It has been shown that pre-positioning diverse MERs before natural disasters could be a viable and economical means to enhance emergency preparedness capability of critical infrastructure systems [5].

MPSs can be called up rapidly and flexibly allocated in appropriate locations to expedite load restoration. Therefore, a growing body of literature [4], [17], [18], [19], [20] has investigated pre-positioning approaches of MPSs for system resilience enhancement. For example, a stochastic pre-positioning model for repair crews and MEGs was presented in [4], and a two-stage pre-positioning framework was designed in [17] to route and schedule MPSs. Electric bus is also leveraged as a generation resource to supply critical loads under natural disasters, and pre-hurricane electric bus allocation was studied in [3] and [21]. However, a majority of the prior works primarily focused on the distribution system and overlooked the impact of dynamic traffic conditions on the travel of MPSs during the recovery process. To bridge the gap, a road network damage/congestion model was considered in [22], and the transportation network was optimized in [23] to arrange a fast route for mobile devices in emergency operations. Nevertheless, these works have not incorporated the negative impact of road flooding incurred by extreme rainfalls on the transportation system. Road flooding could significantly prolong the vehicle travel time and profoundly impede the dispatch of MPSs during service restoration. Since EDVs can effectively mitigate road flooding, coordinated pre-positioning of MPSs and EDVs could be a promising solution for the ETN, which has not been well explored in previous studies.

Pre-positioning plans entail sufficient robustness to handle uncertainties in rainfall-induced disasters that could dramatically impact the recovery process of the ETN under extreme rainfalls. Stochastic programming and robust optimization are widely used approaches for handling uncertain variables [3], [4], [17], [18], [19], [20], [21], [22]. Stochastic programming requires accurate probability distribution functions of the uncertain variables to generate post-disaster scenarios and is computationally expensive when having a large number of scenarios [24]. In contrast, robust optimization only requires limited information about the uncertainties and is more computationally tractable, especially for problem under extreme disaster conditions. Moreover, to the best of the authors' knowledge, existing works have not considered uncertainties in line outages and flooded roads that commonly occur in the ETN under extreme rainfalls. Hence, pre-positioning MPSs and EDVs in a robust optimization manner considering uncertainties in line outages and flooded roads is a promising strategy for resilience enhancement of the ETN confronted with extreme rainfalls.

C. Research Contribution

In this article, a robust EPP scheme is proposed to enhance the proactive emergency preparedness and resilience of the ETN, by considering uncertainties in line outages and flooded roads under extreme rainfalls. The pivotal contributions of this article are threefold as follows:

1) A risk identification approach based on rainfall-runoff simulation is developed to locate flood-prone transportation roads. A coupled 1D-2D hydrodynamic model with hyperbolic partial differential equations is formed to simulate the dynamic flooding process for obtaining the spatio-temporal distribution of road inundation depth. Therefore, the diverse MER routing with the vehicle travel time can be estimated based on a speed attenuation function and flood-prone road identification.
2) A tri-level robust EPP model is developed to minimize the worst-case load curtailment for resilience enhancement of the ETN against extreme rainfalls. The upper level aims to pre-position MPSs and EDVs and perform proactive network reconfiguration before rainstorms to boost emergency preparedness capability. Under the worst uncertainty realization from the middle level, the lower level strives to coordinate the optimal MER routing and dispatch with the post-disaster network reconfiguration for expediting service restoration.
3) A tailored solution method based on the nested column-and-constraint generation (NC&CG) algorithm is devised

Authorized licensed use limited to: Univ of Texas at Dallas. Downloaded on January 21,2024 at 03:38:14 UTC from IEEE Xplore. Restrictions apply.

to decompose the tri-level problem into a pre-disaster preparedness master problem and a post-disaster restoration subproblem, in order to iteratively achieve the optimal emergency preparedness plan. Multiple linearization techniques are employed to cope with the inherent nonlinearities within bilinear terms, quadratic constraints of capacity limits, and hyperbolic tangent functions to recast the proposed nonlinear EPP model into a tractable mixed-integer linear programming (MILP) problem.

The remainder of the article is organized as follows. Section II introduces the risk identification approach of flood-prone roads and details the tri-level robust EPP model. Section III presents a tailored solution method for solving the EPP model. Section IV demonstrates the numerical results and analysis on a modified IEEE 33-bus distribution network and 30-node transportation network. Section V concludes this article.

II. Problem Formulation

A. Risk Identification of Flood-Prone Roads

Rainfall drops onto impervious roads, forms surface runoff, and flows into underground drainage networks via stormwater manholes. If excess rainwater cannot be drained rapidly, the transportation system will suffer from road flooding [25]. Our proposed risk identification approach first simulates the rainfall-runoff process to obtain the inundation depth on each road. One-dimensional Saint-Venant equations (1D SVEs) are utilized to describe the water flow through drainage pipes, formulated as (1a). Two-dimensional shallow water equations (2D SWEs) are adopted to describe the runoff on road surfaces [26], which can be written in a conservative vector form as (1b). Moreover, the 2D SWEs and the 1D SVEs are linked by exchanging boundary information and source terms at the junction sections. Therefore, they can be utilized to construct a coupled 1D-2D hydrodynamic model for simulating the dynamic flooding process [27], [28]. A finite difference method with the Preissmann implicit scheme is typically used to solve the 1D SVEs, and a finite volume method with the Godunov-type scheme could be adopted to solve the 2D SWEs [26], [28]. Geospatial information and forecasted rainfall distribution are needed for the rainfall-runoff simulation. More details of the coupled model could be found in [26], [27], [28]. Then, the spatial-temporal distribution of road inundation depth can be obtained after the rainfall-runoff simulation. A road is considered flood-prone if its maximum inundation depth exceeds a threshold set as 0.15 meters in this article.

$$\begin{cases} \partial_t A + \partial_x Q = S_{\mathrm{r}} \\ \partial_t Q + \partial_x (Q^2/A) + gA\partial_x H = gA(S_{\mathrm{b}} - S_{\mathrm{f}}) \end{cases} \tag{1a}$$

$$\partial_t \mathbf{U}(H, q_x, q_y) + \partial_x \mathbf{F}(\mathbf{U}) + \partial_y \mathbf{G}(\mathbf{U}) = \mathbf{S} \tag{1b}$$

where x, y, and t are the spatial and temporal coordinates; A is the wetted area; Q is the the flow discharge rate; S_{r} is the lateral inflow per unit length; S_{b} is the friction slope; S_{f} is the bed slope; g is the gravitational acceleration; $\mathbf{U}$ is the vector of the conserved variables; $\mathbf{F}$ is the flux vector; $\mathbf{S}$ is the source term vector; q_x and q_y are the unit discharges in x and y direction, respectively; H is the water depth.

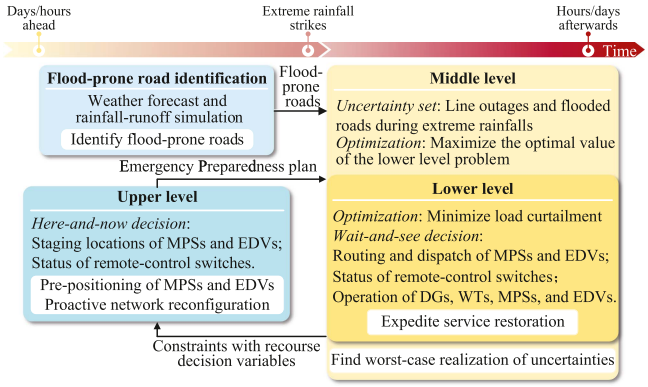

Fig. 1. Overall framework of the proposed tri-level robust EPP model.

As the inundation depth increases and the running speed decreases, the travel time will be significantly extended [25]. Traffic disruption occurs when the inundation depth reaches a critical threshold. Some studies, such as [6], adopted a semi-dynamic traffic assignment model to describe traffic flow distribution for estimating the travel time on each road. This model must satisfy a constraint that the duration of each period should be longer than the maximum travel time on the used routes [29]. However, extended travel time, due to road flooding, probably violates this constraint, making this model inapplicable to transportation network modeling under extreme rainfalls. Moreover, it is assumed in this article that most of the vehicles, except for emergency vehicles, will take refuge in public shelters before extreme rainfalls occur. Therefore, the travel time on a flooded road is not affected by the traffic flow distribution and mainly depends on the inundation depth. A speed attenuation function proposed in [27] could link the inundation depth H_r with the running speed v_r on a flooded road r to enable travel time estimation for MPSs and EDVs, formulated as

$$v_r = \frac{\tilde{v}_r}{2} \tanh\left(\frac{-H_r + a}{b}\right) + \frac{\tilde{v}_r}{2} \tag{2a}$$

where $\tilde{v}_r$ is the design speed on road r; a is the median of the critical depth that causes traffic disruptions; b is an elastic attenuation coefficient. It is assumed that each MPS and EDV would travel on road r at the running speed v_r. Then, the travel time T_r on road r with lengh L_r can be calculated by

$$T_r = L_r/v_r = 1/\left[\frac{1}{2\tilde{T}_r} \tanh\left(\frac{-H_r + a}{b}\right) + \frac{1}{2\tilde{T}_r}\right] \tag{2b}$$

where $\tilde{T}_r = L_r/\tilde{v}_r$ is the free travel time on road r.

B. Framework of Tri-Level EPP Model

For handling the intrinsic uncertainties associated with line outages and flooded roads during extreme rainfalls, the EPP model is formulated as a tri-level robust optimization problem, and Fig. 1 illustrates the overall framework of the EPP model. The upper level optimization determines the staging locations of MPSs and EDVs and proactively reconfigures the distribution network into a less affected state ahead of extreme rainfalls. The upper-level variables are regarded as *here-and-now* decisions,

Authorized licensed use limited to: Univ of Texas at Dallas. Downloaded on January 21,2024 at 03:38:14 UTC from IEEE Xplore. Restrictions apply.

since they are decided prior to the realization of uncertainties and remain fixed in the middle and lower levels. Under any realization of uncertainties, the lower level optimization dispatches MPSs from staging locations to buses available for MPS connection via appropriate routes, to coordinate with the post-disaster network reconfiguration for expediting service restoration. In addition, the lower level optimization dispatches EDVs to flooded roads to decrease inundation depth, thereby reducing the travel time of MPSs. The objective of the lower level optimization is to minimize the load curtailment, and the corresponding variables are regarded as *wait-and-see* decisions since they are optimized after the realization of uncertainties. The worst-case realization of uncertainties is identified from the middle level optimization by maximizing the optimal value of the lower level problem. Then, its corresponding constraints with recourse decision variables are generated and added to the upper level problem.

C. Upper-Level Optimization Constraints

The relevant constraints for the pre-positioning of MPSs and EDVs are presented as (3a)–(3c), where (3a) guarantees that each MPS and EDV should be pre-positioned exactly in one staging location; (3b) ensures that all of MPSs and EDVs should be pre-positioned before extreme rainfall occurs; (3c) imposes the total number of MPSs and EDVs pre-positioned in staging location g that cannot violate the allowable maximum number. In this article, it is assumed that each MPS or EDV carries enough fuel and each MESS is fully charged.

$$\sum_{t\in\mathcal{T}}\sum_{g\in\mathcal{G}}\gamma_{i,t}^{\mathrm{v}_i g}=1 \quad \forall i\in\mathcal{V} \tag{3a}$$

$$\sum_{t\in\mathcal{T}}\gamma_{i,t}^{\mathrm{v}_i g}(t+T_t^{\mathrm{v}_i g})\le T_{\mathrm{ER}} \quad \forall g\in\mathcal{G}, i\in\mathcal{V} \tag{3b}$$

$$\sum_{t\in\mathcal{T}}\sum_{i\in\mathcal{V}}\gamma_{i,t}^{\mathrm{v}_i g}\le K_g \quad \forall g\in\mathcal{G} \tag{3c}$$

Before the extreme rainfall, the distribution network can be proactively reconfigured by remote-control switches (RCSs) to prepare for the post-event network reconfiguration. A linearized branch flow model [30] is adopted to represent the ac power flow in a radial distribution network. The constraints pertaining to power flow equations, line capacity limits, and operation limits of distributed generators (DGs) and wind turbines (WTs) [24], [31], [32], are given by (4a)–(4i). Constraint (4a) indicates that if a line is closed, one end of the line must be the parent of the other end. Constraints (4b) and (4c) limit the active and reactive power injections at each bus. Constraint (4d) shows the relationship between the voltage drop and power flow of each line considering the line closed/open state. Constraints (4e)–(4g) enforce capacity limits on lines, DGs, and WTs. Constraint (4h) ensures the active power outputs of DGs and WTs are non-negative, and the power outputs of WTs cannot exceed the predicted generation. Constraint (4i) enforces the ramping up/down limit on each DG. Other constraints pertaining to radial structure limits, voltage limits, and power balance limits can be found in [4].

$$\alpha_{ij,t}=\beta_{ij,t}+\beta_{ji,t} \quad \forall(i,j)\in\mathcal{L}, t\in\mathcal{T} \tag{4a}$$

$$P_{i,t}^{\mathrm{in}}=P_{i,t}^{\mathrm{mg}}+P_{i,t}^{\mathrm{dg}}+P_{i,t}^{\mathrm{wt}}-P_{i,t} \quad \forall i\in\mathcal{B}, t\in\mathcal{T} \tag{4b}$$

$$Q_{i,t}^{\mathrm{in}}=Q_{i,t}^{\mathrm{mg}}+Q_{i,t}^{\mathrm{dg}}+Q_{i,t}^{\mathrm{wt}}-Q_{i,t} \quad \forall i\in\mathcal{B}, t\in\mathcal{T} \tag{4c}$$

$$\begin{aligned}2(r_{ij}P_{ij,t}+x_{ij}Q_{ij,t})+(\alpha_{ij,t}-1)M\le V_{i,t}-V_{j,t}\le 2(r_{ij}P_{ij,t}\\ +x_{ij}Q_{ij,t})+(1-\alpha_{ij,t})M \quad \forall(i,j)\in\mathcal{L}, t\in\mathcal{T}\end{aligned} \tag{4d}$$

$$P_{ij,t}^2+Q_{ij,t}^2\le\alpha_{ij,t}\bar{S}_{ij}^2 \quad \forall(i,j)\in\mathcal{L}, t\in\mathcal{T} \tag{4e}$$

$$(P_{i,t}^{\mathrm{dg}})^2+(Q_{i,t}^{\mathrm{dg}})^2\le(\bar{S}_i^{\mathrm{dg}})^2 \quad \forall i\in\mathcal{B}, t\in\mathcal{T} \tag{4f}$$

$$(P_{i,t}^{\mathrm{wt}})^2+(Q_{i,t}^{\mathrm{wt}})^2\le(\bar{S}_i^{\mathrm{wt}})^2 \quad \forall i\in\mathcal{B}, t\in\mathcal{T} \tag{4g}$$

$$0\le P_{i,t}^{\mathrm{wt}}\le\bar{P}_{i,t}^{\mathrm{wt}},\ 0\le P_{i,t}^{\mathrm{dg}} \quad \forall i\in\mathcal{B}, t\in\mathcal{T} \tag{4h}$$

$$|P_{i,t}^{\mathrm{dg}}-P_{i,t-\Delta T}^{\mathrm{dg}}|\le P_i^{\mathrm{rp}} \quad \forall i\in\mathcal{B}, t\in\mathcal{T} \tag{4i}$$

D. Uncertainty Set Construction in Middle Level Optimization

Generally, after extreme rainfall occurs, the repair crews will be dispatched to repair the damaged lines and restore them to a serviceable state. The crew dispatch is beyond the scope of this article, and it is assumed that once line (i,j) is damaged, the nearby crews will repair it with a time of $\Delta T_{ij}^{\mathrm{d}}$, and then the line at subsequent periods will remain in a serviceable state. It is assumed for simplicity that only road $r\in\mathcal{R}_{\mathrm{fp}}$ may be flooded during extreme rainfalls, and all lines are in the serviceable state before extreme rainfalls. Consequently, the uncertainties of line outages and flooded roads are described by the uncertainty set $\tilde{\mathcal{U}}$, as follows.

$$\tilde{\mathcal{U}}:=\left\{(\delta_{ij},\phi_{ij,t'},\psi_r)\ \middle|\ \Psi_1\le\sum_{r\in\mathcal{R}_{\mathrm{fp}}}\psi_r\le\Psi_2\right. \tag{5a}$$

$$\Phi_1\le\sum_{(i,j)\in\mathcal{L}}\delta_{ij}\le\Phi_2 \tag{5b}$$

$$\sum_{t'\in\mathcal{T}'}|\phi_{ij,t'}-\phi_{ij,t'-\Delta T}|\le 2, \forall(i,j)\in\mathcal{L} \tag{5c}$$

$$\left.\sum_{t'\in\mathcal{T}'}(1-\phi_{ij,t'})=\delta_{ij}\lceil\Delta T_{ij}^{\mathrm{d}}/\Delta T\rceil, \forall(i,j)\in\mathcal{L}\right\} \tag{5d}$$

E. Lower-Level Optimization Constraints

For convenience, "node" and "location" are used interchangeably in this article. The fictitious roads are introduced to connect nodes to themselves for ease of modeling. Constraints (6a)–(6o) are applied for the routing and dispatch of MPSs and EDVs, and are valid for all $t'\in\mathcal{T}'$. (6a)–(6c) are used to estimate the travel time on each road. (6d) links the travel time of routes and roads. (6e) implies that MPSs and EDVs can be dispatched to other nodes from staging location g after rainfalls occur only if they were pre-positioned at staging location g before rainfalls. (6f) and (6g) impose that MPSs and EDVs should be dispatched from staging locations to other locations after the rainfall strikes. (6h) points out that the time EDV i arrives at node j from g is

Authorized licensed use limited to: Univ of Texas at Dallas. Downloaded on January 21,2024 at 03:38:14 UTC from IEEE Xplore. Restrictions apply.

equal to the departure time plus the travel time. (6i) shows that an EDV can decrease the inundation depth of a flooded road if it arrives at either end of this road. (6j) ensures that once an EDV arrives at a flooded road, it remains available on the road in the subsequent time. (6k) imposes the limits on the drainage capacities of EDVs, and (6l) guarantees that the inundation depth is non-negative. Let $\langle j \rangle$ be the bus that can be connected with MPSs located at $j \in \mathcal{N}_{\rm ac}$, (6m) illustrates that if an MPS is dispatched from node g to j and installed to the bus $\langle j \rangle$, the required time is equal to the departure time plus the travel time and the time used for connecting to the bus. (6n) is similar to (6j). (6o) indicates that the total capacities of MPSs connected to bus $\langle j \rangle$ cannot exceed the allowable maximum capacity.

$$T_{r,t'} = 0 \quad \forall r \in \mathcal{R}_{\rm f}, t' \in T' \tag{6a}$$

$$T_{r,t'} = T_r^0 \quad \forall r \in \mathcal{R} \backslash \mathcal{R}_{\rm fp} \tag{6b}$$

$$T_{r,t'} = 1/\left[\frac{1}{2\tilde{T}_r}\tanh\left(\frac{-H_{r,t'}+a}{b}\right)+\frac{1}{2\tilde{T}_r}\right] \quad \forall r \in \mathcal{R}_{\rm fp} \tag{6c}$$

$$T_{k,t'}^{gj} = \sum_{r \in \mathcal{R} \cup \mathcal{R}_{\rm f}} T_{r,t'} \delta_{r,k}^{gj} \quad \forall k \in \mathcal{K}_{gj}, g \in \mathcal{G}, j \in \mathcal{N}_{\rm ac} \cup \mathcal{N}_{\rm f} \tag{6d}$$

$$\sum_{t \in \mathcal{T}} \gamma_{i,t}^{{\rm v}_i g} \geq \sum_{t' \in \mathcal{T}'} \sum_{j \in \mathcal{N}_{\rm ac(f)}} \sum_{k \in \mathcal{K}_{gj}} \gamma_{i,k,t'}^{gj} \quad \forall g \in \mathcal{G}, i \in \mathcal{V}_{\rm P(D)} \tag{6e}$$

$$\sum_{t' \in \mathcal{T}'} \sum_{g \in \mathcal{G}} \sum_{j \in \mathcal{N}_{\rm ac(f)}} \sum_{k \in \mathcal{K}_{gj}} \gamma_{i,k,t'}^{gj} = 1 \quad \forall i \in \mathcal{V}_{\rm P(D)} \tag{6f}$$

$$\sum_{t' \in \mathcal{T}'} \sum_{j \in \mathcal{N}_{\rm ac(f)}} \xi_{i,t'}^{j} = 1 \quad \forall i \in \mathcal{V}_{\rm P(D)} \tag{6g}$$

$$\sum_{t' \in \mathcal{T}'} \sum_{g \in \mathcal{G}} \sum_{k \in \mathcal{K}_{gj}} \gamma_{i,k,t'}^{gj}(t' + T_{k,t'}^{gj}) \leq \sum_{t' \in \mathcal{T}'} t' \xi_{i,t'}^{j} \leq \Delta T - \varepsilon + \sum_{t' \in \mathcal{T}'} \sum_{g \in \mathcal{G}} \sum_{k \in \mathcal{K}_{gj}} \gamma_{i,k,t'}^{gj}(t' + T_{k,t'}^{gj}) \quad \forall i \in \mathcal{V}_{\rm D}, j \in \mathcal{N}_{\rm f} \tag{6h}$$

$$H_{r,t'} = H_{r,t'-\Delta T} + \psi_r(h_{r,t'} - h_{r,t'-\Delta T}) - \sum_{i \in \mathcal{V}_{\rm D}} \sum_{j \in end(r)} d_{i,t'}^{j} \quad \forall r \in \mathcal{R}_{\rm fp} \tag{6i}$$

$$z_{i,t'}^{j} = \sum_{t''=T_0'}^{t'} \xi_{i,t''}^{j} \quad \forall i \in \mathcal{V}_{\rm D}, j \in \mathcal{N}_{\rm f} \tag{6j}$$

$$0 \leq d_{i,t'}^{j} \leq z_{i,t'}^{j} \bar{d}_i \quad \forall i \in \mathcal{V}_{\rm D}, j \in \mathcal{N}_{\rm f} \tag{6k}$$

$$0 \leq H_{r,t'} \quad \forall r \in \mathcal{R}_{\rm fp}, t' \in \mathcal{T}' \tag{6l}$$

$$\sum_{t' \in \mathcal{T}'} \sum_{g \in \mathcal{G}} \sum_{k \in \mathcal{K}_{gj}} \gamma_{i,k,t'}^{gj}(t' + T_i^{\rm co} + T_{k,t'}^{gj}) \leq \sum_{t' \in \mathcal{T}'} t' \xi_{i,t'}^{j} \leq \sum_{t' \in \mathcal{T}'} \sum_{g \in \mathcal{G}} \sum_{k \in \mathcal{K}_{gj}} \gamma_{i,k,t'}^{gj}(t' + T_i^{\rm co} + T_{k,t'}^{gj}) + \Delta T - \varepsilon \quad \forall i \in \mathcal{V}_{\rm P}, j \in \mathcal{N}_{\rm ac} \tag{6m}$$

$$u_{i,t'}^{\langle j \rangle} = \sum_{t''=T_0'}^{t'} \xi_{i,t''}^{j} \quad \forall i \in \mathcal{V}_{\rm P}, j \in \mathcal{N}_{\rm ac} \tag{6n}$$

$$\sum_{i \in \mathcal{V}_{\rm G}} u_{i,t'}^{\langle j \rangle} \bar{P}_i^{\rm G} + \sum_{i \in \mathcal{V}_{\rm S}} u_{i,t'}^{\langle j \rangle} \bar{P}_i^{\rm S} \leq C_{\langle j \rangle} \quad \forall j \in \mathcal{N}_{\rm ac} \tag{6o}$$

The power output of MEG $a \in \mathcal{V}_{\rm G}$ is constrained by (7) ($\forall t' \in \mathcal{T}'$), and the operating constraints of MESS $b \in \mathcal{V}_{\rm S}$ are shown in (8) ($\forall t' \in \mathcal{T}'$) [24], [33], [34].

$$\begin{cases} 0 \leq P_{a,\langle j \rangle,t'}^{\rm G} \leq u_{a,t'}^{\langle j \rangle} \bar{P}_a^{\rm G} \\ -u_{a,t'}^{\langle j \rangle} \bar{Q}_a^{\rm G} \leq Q_{a,\langle j \rangle,t'}^{\rm G} \leq u_{a,t'}^{\langle j \rangle} \bar{Q}_a^{\rm G} \end{cases} \tag{7}$$

$$\begin{cases} \sum_{j \in \mathcal{N}_{\rm ac}} P_{b,\langle j \rangle,t'}^{\rm S} = P_{b,t'}^{\rm Sd} - P_{b,t'}^{\rm Sc} \\ -u_{b,t'}^{\langle j \rangle} \bar{P}_b^{\rm S} \leq P_{b,\langle j \rangle,t'}^{\rm S} \leq u_{b,t'}^{\langle j \rangle} \bar{P}_b^{\rm S} \\ SoC_{b,t'} = SoC_{b,t'-\Delta T} - (P_{b,t'}^{\rm Sd}/\eta_b^{\rm Sd} - P_{b,t'}^{\rm Sc}\eta_b^{\rm Sc})\Delta T \\ 0 \leq P_{b,t'}^{\rm Sd} \leq \mu_{b,t'}^{\rm Sd} \bar{P}_b^{\rm S}, 0 \leq P_{b,t'}^{\rm Sc} \leq \mu_{b,t'}^{\rm Sc} \bar{P}_b^{\rm S} \\ \mu_{b,t'}^{\rm Sd} + \mu_{b,t'}^{\rm Sc} \leq 1, \ \underline{SoC}_b \leq SoC_{b,t'} \leq \overline{SoC}_b \end{cases} \tag{8}$$

Moreover, the post-disaster network reconfiguration is performed to coordinate with the dispatch of MPSs. Due to space limits, (4f)–(4i) are used as partial operating constraints of the distribution network in the lower level. The symbols t and T in these constraints are replaced by t' and T', respectively. The rest of the operating constraints are formulated as follows and are valid for all $t' \in \mathcal{T}'$.

$$\alpha_{ij,t'} \phi_{ij,t'} = \beta_{ij,t'} + \beta_{ji,t'} \quad \forall (i,j) \in \mathcal{L} \tag{9a}$$

$$P_{ij,t'}^2 + Q_{ij,t'}^2 \leq \alpha_{ij,t'} \phi_{ij,t'} \bar{S}_{ij}^2 \quad \forall (i,j) \in \mathcal{L} \tag{9b}$$

$$0 \leq \Delta P_{i,t'} \leq P_{i,t'} \quad \forall i \in \mathcal{B} \tag{9c}$$

$$\Delta Q_{i,t'} = \Delta P_{i,t'} Q_{i,t'}/P_{i,t'} \quad \forall i \in \mathcal{B} \tag{9d}$$

$$V_{i,t'} - V_{j,t'} \leq 2(r_{ij}P_{ij,t'} + x_{ij}Q_{ij,t'}) + (2 - \alpha_{ij,t'} - \phi_{ij,t})M \quad \forall (i,j) \in \mathcal{L} \tag{9e}$$

$$V_{i,t'} - V_{j,t'} \geq 2(r_{ij}P_{ij,t'} + x_{ij}Q_{ij,t'}) + (\alpha_{ij,t'} + \phi_{ij,t} - 2)M \quad \forall (i,j) \in \mathcal{L} \tag{9f}$$

$$P_{i,t'}^{\rm in} = P_{i,t'}^{\rm mg} + P_{i,t'}^{\rm dg} + P_{i,t'}^{\rm wt} + \sum_{a \in \mathcal{V}_{\rm G}} P_{a,i,t'}^{\rm G} + \sum_{b \in \mathcal{V}_{\rm S}} P_{b,i,t'}^{\rm S} - (P_{i,t'} - \Delta P_{i,t'}) \quad \forall i \in \mathcal{B} \tag{9g}$$

$$Q_{i,t'}^{\rm in} = Q_{i,t'}^{\rm mg} + Q_{i,t'}^{\rm dg} + Q_{i,t'}^{\rm wt} + \sum_{a \in \mathcal{V}_{\rm G}} Q_{a,i,t'}^{\rm G} - (Q_{i,t'} - \Delta Q_{i,t'}) \quad \forall i \in \mathcal{B} \tag{9h}$$

F. Formulation of Tri-Level Robust EPP Model

Let $\tilde{\boldsymbol{u}}$ denote the uncertainty variables, i.e., $\tilde{\boldsymbol{u}} = \{[\delta_{ij}]_{(i,j)\in\mathcal{L}}, [\phi_{ij,t'}]_{(i,j)\in\mathcal{L},t'\in\mathcal{T}'}, [\psi_r]_{r\in\mathcal{R}_{\rm fp}}\}$. Similarly, the upper-level and lower-level decision variables are denoted with $\tilde{\boldsymbol{x}}$ and $\tilde{\boldsymbol{y}}$, respectively. Based on the discussion in Section II-B, the tri-level robust EPP model is formulated as:

$$\min_{\tilde{\boldsymbol{x}}} \max_{\tilde{\boldsymbol{u}} \in \tilde{\mathcal{U}}} \min_{\tilde{\boldsymbol{y}}} \sum_{t' \in \mathcal{T}'} \sum_{i \in \mathcal{B}} \omega_i \Delta P_{i,t'} \Delta T$$
$$\text{s.t.} \ \ (3a)-(4i), (6a)-(9h). \tag{10}$$

The sum of the road inundation depth is added to the objective function with a small weight coefficient to ensure that EDVs can

Authorized licensed use limited to: Univ of Texas at Dallas. Downloaded on January 21,2024 at 03:38:14 UTC from IEEE Xplore. Restrictions apply.

continuously decrease inundation depth. It is computationally intractable to solve the optimization problem in (10) due to the nonlinear constraints (5c), (6c), (6h), (6m), (9a) and (9b). Moreover, (4e)–(4g) enable the construction of the dual problem for the lower level problem to be thorny. Therefore, a tailored solution method is developed in the following section for solving the optimization problem in (10).

III. Solution Methodology

In this section, the proposed solution method recasts the optimization problem in (10) into a computationally tractable MILP problem, by leveraging multiple linearization techniques, and then iteratively solves the MILP problem by the NC&CG algorithm [35].

a) Piecewise Linear Approximation of Univariate Nonlinear Function: Constraint (6c) constains a hyperbolic tangent function, indicating that $T_{r,t'}$ is a univariate nonlinear function of $H_{r,t'}$, which can be linearized by piecewise linear approximation [36]. The boundary $[0, \overline{H}]$ of $H_{r,t'}$ is uniformly partitioned into N intervals, i.e., $[H_{n-1}, H_n]$, $\forall n \in \{1, \ldots, N\}$, and the curve is approximately replaced by a straight line in each interval. By introducing auxiliary variables $w'_{n,r,t'} \in [0,1]$ assigned to H_n, and $w''_{n,r,t'} \in \{0,1\}$ assigned to partition n, constraint (6c) is replaced by:

$$H_{r,t'} = \sum_{n=0}^{N} w'_{n,r,t'} H_n,\ T_{r,t'} = \sum_{n=0}^{N} w'_{n,r,t'} T_r(H_n) \tag{11a}$$

$$w'_{0,r,t'} \le w''_{0,r,t'},\ w'_{N,r,t'} \le w''_{N-1,r,t'} \tag{11b}$$

$$w'_{n,r,t'} \le w''_{n-1,r,t'} + w''_{n,r,t'}\ \forall n \in \{1, \ldots, N-1\} \tag{11c}$$

$$\sum_{n=0}^{N} w'_{n,r,t'} = 1,\ \sum_{n=0}^{N-1} w''_{n,r,t'} = 1 \tag{11d}$$

b) Polygon Approximation of Quadratic Constraints: The linearization of constraint (4e) is introduced as an example, and the same procedures are applied to (4f), (4g), and (9b). The feasible region defined by (4e) is represented by a circular area which can be approximated by the region of an equilateral polygon inscribed in the circle [37]. The polygonal area is bounded by N_{qc} line segments. Let c_{1n} and c_{2n} be the slope and y-intercept of line segment $n \in \{1, \ldots, N_{\text{qc}}\}$, the set of line segments with positive y-intercept is defined as A^+, and the set with negative y-intercept is defined as A^-. Consequently, (4e) is linearized as (12).

$$\begin{cases} P_{ij,t} - c_{1n} Q_{ij,t} - c_{2n} \le 0 & \forall n \in A^+ \\ P_{ij,t} - c_{1n} Q_{ij,t} - c_{2n} \ge 0 & \forall n \in A^- \\ -S_{ij}\alpha_{ij,t} \le P_{ij,t} \le S_{ij}\alpha_{ij,t} \\ -S_{ij}\alpha_{ij,t} \le Q_{ij,t} \le S_{ij}\alpha_{ij,t} \end{cases} \tag{12}$$

c) Equivalent Linearization of absolute value and bilinear terms: Constraint (5c) contains an absolute value term $|\phi_{ij,t'} - \phi_{ij,t'-\Delta T}|$. Constraints (6h) and (6m) contains a bilinear term $\gamma^{gj}_{i,k,t} T^{gj}_{k,t'}$, and constraint (9a) contains a bilinear term $\alpha_{ij,t'}\phi_{ij,t'}$. By introducing an auxiliary binary variable $\lambda_{ij,t'}$, constraint (9a) can be reformulated as (13). Using the big-M method with different forms [6], [36], constraint (5c) can be transformed into (14), and the bilinear term $\gamma^{gj}_{i,k,t'} T^{gj}_{k,t'}$ can be linearized as (15).

$$\begin{cases} \lambda_{ij,t'} = \beta_{ij,t'} + \beta_{ji,t'},\ \lambda_{ij,t'} \le \alpha_{ij,t'} \\ \lambda_{ij,t'} \le \phi_{ij,t'},\ \lambda_{ij,t'} \ge \alpha_{ij,t'} + \phi_{ij,t'} - 1 \end{cases} \tag{13}$$

$$\begin{cases} \sum_{t' \in \mathcal{T}} \zeta_{ij,t'} \le 2 \\ \phi_{ij,t'} - \phi_{ij,t'-\Delta T} \le \zeta_{ij,t'},\ \phi_{ij,t'-\Delta T} - \phi_{ij,t'} \le \zeta_{ij,t'} \\ \zeta_{ij,t'} \le \phi_{ij,t'} - \phi_{ij,t'-\Delta T} + (1 - \kappa_{ij,t'})M \\ \zeta_{ij,t'} \le \phi_{ij,t'-\Delta T} - \phi_{ij,t'} + \kappa_{ij,t'} M \end{cases} \tag{14}$$

$$\begin{cases} \varpi^{gj}_{i,k,t'} \le \gamma^{gj}_{i,k,t'} M,\ \varpi^{gj}_{i,k,t'} \le T^{gj}_{k,t'} \\ \varpi^{gj}_{i,k,t'} \ge T^{gj}_{k,t'} - (1 - \gamma^{gj}_{i,k,t'})M,\ \varpi^{gj}_{i,k,t'} \ge 0 \end{cases} \tag{15}$$

where $\zeta_{ij,t'}$ and $\kappa_{ij,t'}$ are auxiliary binary variables; $\varpi^{gj}_{i,k,t'}$ is an auxiliary continuous variable. Note that $\varpi^{gj}_{i,k,t'}$ replaces $\gamma^{gj}_{i,k,t'} T^{gj}_{k,t'}$ in (6h) and (6m).

After linearization of the nonlinear constraints, the upper-level variables and uncertainty variables are denoted with $\boldsymbol{x}$ and $\boldsymbol{u}$, respectively. Let $\mathcal{U}$ denote the linearized uncertainty set. Moreover, the lower-level variables are divided into continuous variables denoted as $\boldsymbol{y}$ and binary variables denoted as $\boldsymbol{z}$. The opitmization problem in (10) is reformulated as an MILP problem that can be written in the following matrix form:

$$\begin{aligned} &\min_{\boldsymbol{x}} \max_{\boldsymbol{u} \in \mathcal{U}} \min_{\boldsymbol{y},\boldsymbol{z}} \mathbf{f}\boldsymbol{y} \\ &\text{s.t. } \mathbf{A}\boldsymbol{x} \le \mathbf{a}, \mathbf{F}\boldsymbol{z} \le \mathbf{c}, \\ &\quad \mathbf{B}\boldsymbol{x} + \mathbf{C}\boldsymbol{u} + \mathbf{D}\boldsymbol{y} + \mathbf{E}\boldsymbol{z} \le \mathbf{b} : \boldsymbol{\pi}. \end{aligned} \tag{16}$$

where $\mathbf{A}$, $\mathbf{B}$, $\mathbf{C}$, $\mathbf{D}$, $\mathbf{E}$, and $\mathbf{F}$ are coefficient matrices; $\mathbf{a}$, $\mathbf{c}$, $\mathbf{b}$, and $\mathbf{f}$ are coefficient vectors; $\boldsymbol{\pi}$ is a set of dual variables.

Some traditional algorithms, such as Bender's decomposition and column-and-constraint generation (C&CG), are available to solve tri-level *min-max-min* optimization models [6]. In general, these algorithms need to dualize lower level *min* problems to reformulate bi-level *max-min* problems into computationally tractable single-level *max* problems. However, in this article, the introduced and inherent binary variables in the linearized lower level *min* optimization problem prevent dualization since strong duality does not hold in general MILP problems. Therefore, these algorithms suffer from convergence issues and are inapplicable for solving the problem in (16). The NC&CG algorithm proposed in [35] could exactly solve robust tri-level optimization models with mixed-integer recourse problems in finite iterations by embedding an inner-level C&CG procedure in the traditional single-level C&CG procedure to handle binary variables in lower level *min* problems. Therefore, the NC&CG algorithm is adopted to solve the proposed tri-level EPP problem. The algorithm first decomposes the tri-level problem into a pre-disaster preparedness master problem **MP** shown in (17) and a post-disaster restoration subproblem **SP** that is a bi-level problem formulated in (20). Here, $\hat{\boldsymbol{x}}$ is a solution given from **MP**. Then, **SP** is transformed into an inner master problem **IMP** shown in (18) and an inner subproblem **ISP** shown in (19). Finally, outer-level and inner-level iteration procedures are implemented to solve **MP** and **SP** until convergence. Algorithm 1 summarizes the devised solution method for the proposed

Authorized licensed use limited to: Univ of Texas at Dallas. Downloaded on January 21,2024 at 03:38:14 UTC from IEEE Xplore. Restrictions apply.

Algorithm 1: Solution method for problem in (10).

Initialization: Set S, N, N_{qc}, ε. $k=0$, $LB=-\infty$, $UB=+\infty$;
Linearization: Linearize nonlinear constraints based on a), b) and c). Then, obtain the MILP problem (16);
while $UB-LB>\varepsilon$ **do**
  Solve the following problem **MP**.

$$\textbf{MP}: \min_{\boldsymbol{x},\boldsymbol{y},\boldsymbol{z}} \ \eta \tag{17a}$$
$$\text{s.t.} \ \ \mathbf{A}\boldsymbol{x}\le\mathbf{a}, \tag{17b}$$
$$\eta\ge\mathbf{f}\boldsymbol{y}_l,\ \mathbf{F}\boldsymbol{z}_l\le\mathbf{c},\ \mathbf{B}\boldsymbol{x}_l+\mathbf{C}\boldsymbol{u}_l^*+\mathbf{D}\boldsymbol{y}_l+\mathbf{E}\boldsymbol{z}_l\le\mathbf{b}. \tag{17c}$$

  where $l=1,\ldots,k$. Derive the optimal solution $(\boldsymbol{x}_{k+1}^*,\eta_{k+1}^*,\boldsymbol{y}_1^*,\boldsymbol{z}_1^*\ldots,\boldsymbol{y}_k^*,\boldsymbol{z}_k^*)$ and update $LB=\eta_{k+1}^*$;
  Set $m=0$, $LB1=-\infty$, $UB1=+\infty$;
  while $UB1-LB1>\varepsilon$ **do**
    Solve the following problem **IMP**.

$$\textbf{IMP}: \max_{\boldsymbol{y},\boldsymbol{\pi},\boldsymbol{u}\in\mathcal{U}} \ \theta \tag{18a}$$
$$\text{s.t.} \ \ \theta\le\mathbf{f}\boldsymbol{y}_r,\ \boldsymbol{\pi}_r\le 0,\ \mathbf{D}^\top\boldsymbol{\pi}_r=\mathbf{f}^\top, \tag{18b}$$
$$\mathbf{B}\boldsymbol{x}_{k+1}^*+\mathbf{C}\boldsymbol{u}+\mathbf{D}\boldsymbol{y}_r+\mathbf{E}\boldsymbol{z}_r^*\le\mathbf{b}, \tag{18c}$$
$$(\mathbf{B}\boldsymbol{x}_{k+1}^*+\mathbf{C}\boldsymbol{u}+\mathbf{D}\boldsymbol{y}_r+\mathbf{E}\boldsymbol{z}_r^*-\mathbf{b})^\top\boldsymbol{\pi}_r=0. \tag{18d}$$

    where $r=1,\ldots,m$. Derive the optimal $\boldsymbol{u}$ denoted by $\boldsymbol{u}_{k+1}^*$ and θ denoted by θ_{m+1}^*. Update $UB1=\theta_{m+1}^*$;
    Solve the following problem **ISP**.

$$\textbf{ISP}: \min_{\boldsymbol{y},\boldsymbol{z}} \ \mathbf{f}\boldsymbol{y} \tag{19a}$$
$$\text{s.t.} \ \ \mathbf{F}\boldsymbol{z}\le\mathbf{c}, \tag{19b}$$
$$\mathbf{B}\boldsymbol{x}_{k+1}^*+\mathbf{C}\boldsymbol{u}_{k+1}^*+\mathbf{D}\boldsymbol{y}+\mathbf{E}\boldsymbol{z}\le\mathbf{b}. \tag{19c}$$

    Derive the optimal solution $(\boldsymbol{y}_{m+1}^*,\boldsymbol{z}_{m+1}^*)$ and update $LB1=\max\{LB1,\mathbf{f}\boldsymbol{y}_{m+1}^*\}$. Create variables $\boldsymbol{y}_{m+1}$ and $\boldsymbol{\pi}_{m+1}$ and add constraints (18b)-(18d) with $r=m+1$ to **IMP**. Update $m=m+1$.
  end
  Create variables $(\boldsymbol{y}_{k+1},\boldsymbol{z}_{k+1})$ and add constraint (17c) with $l=k+1$ to **MP**. Update $UB=\min\{UB,UB1\}$ and $k=k+1$.
end
Output: The optimal emergency preparedness plan $\boldsymbol{x}_k^*$.

robust EPP problem in (10).

$$\textbf{SP}: \max_{\boldsymbol{u}\in\mathcal{U}} \min_{\boldsymbol{y},\boldsymbol{z}} \mathbf{f}\boldsymbol{y}$$
$$\text{s.t.} \ \ \mathbf{F}\boldsymbol{z}\le\mathbf{c},\ \mathbf{B}\hat{\boldsymbol{x}}+\mathbf{C}\boldsymbol{u}+\mathbf{D}\boldsymbol{y}+\mathbf{E}\boldsymbol{z}\le\mathbf{b}:\boldsymbol{\pi}. \tag{20}$$

IV. Case Studies

A. Network Data

The proposed robust EPP approach is tested on a modified IEEE 33-bus distribution network with a 30-node transportation network, as illustrated in Fig. 2. Three DGs are installed in the distribution network, and their capacities are set as 5, 4, and 3 MVA. Four WTs are also installed, and their capacities are set as 1, 1, 1.5, and 0.8 MVA. The WT generation and the loads are forecasted based on historical data from Changsha, China. Buses 3, 8, 16, 20, 24, and 30 are selected for connecting MPSs, and their corresponding nodes in the transportation network are 3, 17, 30, 6, 14, and 23, respectively. There are two staging locations for MPSs and EDVs to be pre-positioned, and each can accommodate eight emergency vehicles. Five MEGs numbered from 1 to 5 and two MESSs numbered 1 and 2 can be pre-positioned in the test. The capacities of MEG1-MEG5 are set as 1, 1, 1.5, 0.8, and 0.8 MVA, respectively. The minimum/maximum allowed SoC of MESS1 and MESS2 is set as 0.1/0.9 and 0.06/0.5 MWh, respectively. Eight EDVs numbered from 1 to 8 are assigned with MPSs for coordinated pre-positioning, and $\bar{d}_i$ of each EDV is set as 5 centimeters per time period. All MPSs are initially located at node 27, and all EDVs are located at node 26. The duration of the lower level problem and the time period are selected as 6 h and 0.5 h, respectively. The weather forecast data is obtained from Hunan Meteorological Bureau. Φ_1/Φ_2 and Ψ_1/Ψ_2 can be set according to the rainfall intensity, which are set as 3/8 and 4/7 respectively in this article. The critical depth for traffic disruptions is set as 0.3 meters [27]. Other technical parameters can be accessed from [38]. The proposed robust EPP problem is implemented on PyCharm platform and solved using Gurobi 10.0.

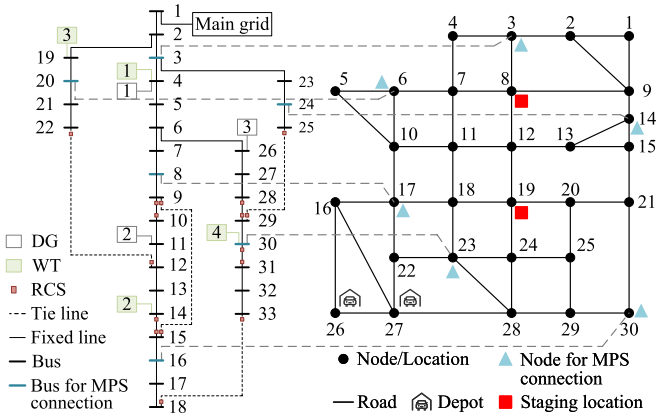

Fig. 2. IEEE 33-bus distribution network and 30-node transportation network.

TABLE I
Flood-Prone Roads and the Maximum Inundation Depth on Them

Road	MID[1]	Road	MID	Road	MID	Road	MID	Road	MID
(3,4)	0.42	(10,11)	0.72	(18,19)	057	(17,22)	0.53	(22,27)	0.60
(6,7)	0.56	(12,13)	0.69	(20,21)	0.57	(24,25)	0.69	(27,28)	0.51
(9,11)	0.66	(10,17)	0.62	(16,26)	0.44	(29,30)	0.65	–	–

[1] MID denotes maximum inundation depth (m)

B. Comparative Results and Analysis

Table I summarizes the identified flood-prone roads and their maximum inundation depth through the study period. It is found that the maximum inundation depth of all flood-prone roads exceeds 0.3 m. Traffic disruptions will occur on these roads unless EDVs are dispatched to them. Three comparative schemes are performed for in-depth analyses to evaluate the effectiveness of the proposed approach: 1) **Scheme 1** is the proposed robust EPP approach for the ETN; 2) **Scheme 2** overlooks the coordination between EDVs and MPSs and separately determines the staging locations of MPSs and EDVs; 3) **Scheme 3** does not perform any emergency preparedness effort. Moreover, constraint (3c) is relaxed in scheme 2 to guarantee that EDVs and MPSs can be pre-positioned equally.

Table II summarizes the decided staging locations for MPSs and EDVs in schemes 1 and 2. As can be seen, compared to

Authorized licensed use limited to: Univ of Texas at Dallas. Downloaded on January 21,2024 at 03:38:14 UTC from IEEE Xplore. Restrictions apply.

TABLE II
PRE-POSITIONING RESULTS WITH SCHEMES 1 AND 2

Scheme	Node 8	Node 19
1	MEG3-5; MESS1,2; EDV1,3,7	MEG1,2; EDV2,4-6,8
2	MEG1-5; MESS1; EDV1,2,5	MESS2; EDV3,4,6-8

TABLE III
RESULTS OF PROACTIVE NETWORK RECONFIGURATION WITH SCHEMES 1 AND 2

Scheme	Closed RCSs	Opened RCSs
1	(9,15), (22,12), (25,28), (30,31)	(9,10), (14,15), (28,29), (18,33)
2	(9,15), (22,12), (25,28), (18,33)	(9,10), (14,15), (28,29), (30,31)

TABLE IV
DAMAGED LINES AND FLOODED ROADS IN A TYPICAL SCENARIO

Damaged lines	Flooded roads
(1,2), (3,4), (11,12), (13,14) (15,16), (19,20), (26,27), (29,30)	(6,7), (9,14), (10,17) (10,11), (12,13), (20,21), (29,30)

TABLE V
DISPATCH RESULTS OF MPSS AND EDVS WITH SCHEMES 1–3

Vehicle	Scheme 1				Scheme 2							Scheme 3					
	Time period (ΔT)				Time period (ΔT)							Time period (ΔT)					
	1	2	3	4-12	1	2	3	4	5	6	7-12	1	2	3	4	5	6-12
MEG1	node 19	→	node 23		node 8	→	node 23					node 27	→	node 23			
MEG2																	
MEG3	node 8	→	node 6		node 8	→	node 6					node 27	→	node 3			
MEG4	node 8	→	node 3		node 8	→	node 3					node 27	→	node 6			
MEG5																	
MESS1												node 27	→	node 3			
MESS2	node 8	→	node 6		node 19	→	node 30										
EDV1	node 8	→	node 7		node 8	→	node 9					node 26	→	node 29			
EDV2	node 19	→	node 12										→	node 9			
EDV3	node 8	→	node 7		node 19	→	node 29						→	node 12			
EDV4	node 19	→	node 20				node 12						→	node 7			
EDV5			node 29		node 8	→	node 7						→	node 20			
EDV6			node 11				node 17							node 17			
EDV7	node 8	→	node 9		node 19	→	node 20						→	node 11			
EDV8	node 19	→	node 17				node 11							node 17			

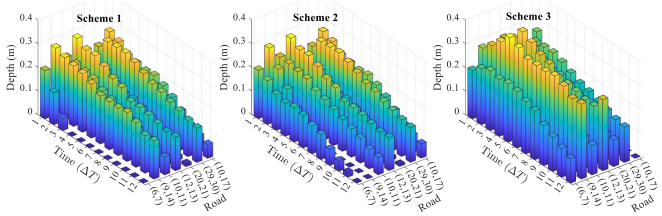

Fig. 3. Inundation depth on flooded roads with schemes 1–3.

scheme 1, most of the MPSs are pre-positioned in node 8 in scheme 2. The pre-positioning results of EDVs in schemes 1 and 2 can be considered the same due to the same parameter $\bar{d}_i$ of each EDV. The results of proactive network reconfiguration with schemes 1 and 2 are summarized in Table III. The switch status of lines (18,31) and (30,31) are opposite, and the rest of the lines equipped with RCSs have the same status. A typical scenario is selected to illustrate the restoration process under the results of schemes 1–3. The damaged lines and flooded roads in this scenario are given in Table IV, and these lines are damaged at $t' = 1$.

The dispatch results of MPSs and EDVs with schemes 1–3 are shown in Table V. Fig. 3 shows the inundation depth on flooded roads at each time period with schemes 1–3. As can be

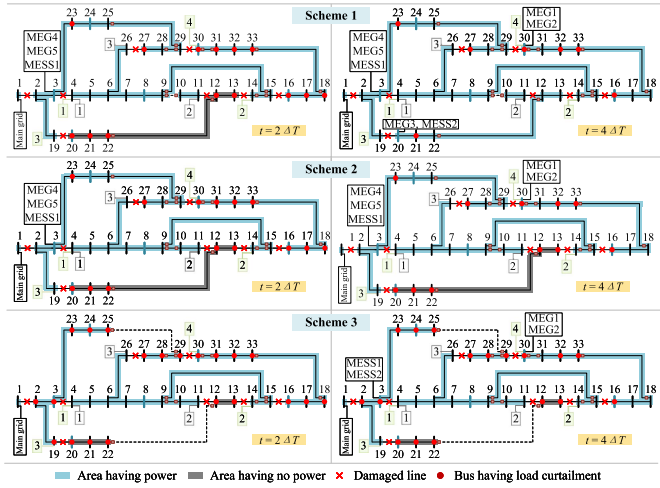

Fig. 4. Distribution network topology and load curtailment at $t' = 2$ and 4 with schemes 1–3.

seen, MPSs are mainly dispatched to nodes 3, 6, and 23 in all three schemes, and MESS2 is dispatched to node 30 in scheme 2. MEG3 is dispatched to node 6 in schemes 1 and 2. Due to the long distance between the depot and the buses that can be connected with MPSs, the inundation depth of flooded roads in scheme 3 is greater than that in schemes 1 and 2. Flooded roads (6,7), (10,17), and (10,11) prevent MEG3 from arriving at node 6. To enable MEG3 to reach node 6 as quickly as possible, EDV1 and EDV3 are coordinately dispatched to node 7 to accelerate the reduction of inundation depth on the flooded road (6,7) in scheme 1. It is seen from Fig. 3 that the inundation depth of road (6,7) decreases to 0.13 m at $t' = 2$, and MEG3 can reach node 6 at $t' = 4$. In scheme 2, only one EDV is dispatched to node 7, and the inundation depth of road (6,7) is 0.19 m at $t' = 2$. Therefore, MEG3 reaches node 6 at $t' = 5$. Only MEG1 and MEG2 reach node 23 at $t' = 3$ in scheme 3, and the rest of the vehicles reach their destination after $t' = 4$. Road flooding and the lack of coordination between MPSs and EDVs prevent MPSs from being connected to the buses timely, resulting in an insufficient power supply and load curtailment.

Fig. 4 depicts the results of network reconfiguration and load curtailment at $t' = 2$ and 4 with schemes 1–3. At $t' = 2$, MEG4, MEG5, and MESS1 arrive at bus 3 for power supply in schemes 1 and 2. In scheme 1, all RCSs are closed except for the RCS on line (9,10), to enable as many buses as possible to be supplied with power. In scheme 3, load curtailment exists at 22 buses since no MPS is connected with the buses at $t' = 2$. In scheme 1, all MPSs are connected at the specified buses, and seven buses have load curtailment at $t' = 4$. Due to the lack of coordination with EDVs in scheme 2, MEG3 and MESS2 cannot be connected at buses 20 and 16 at $t' = 4$, resulting in load curtailment at buses 20, 22, 12, and 13. In scheme 3, MEG3-5 are not connected to buses 3 and 6 timely at $t' = 4$, resulting in load curtailment at 17 buses. Fig. 5 shows the load curtailment at $t' = 9$ and $t' = 12$ in scheme 1. As can be seen, damaged lines (26,27), (1,2), and (15,16) are repaired, and line (25,29) is opened at $t' = 9$ to maintain the radial structure. Load curtailment exists only at bus

Authorized licensed use limited to: Univ of Texas at Dallas. Downloaded on January 21,2024 at 03:38:14 UTC from IEEE Xplore. Restrictions apply.

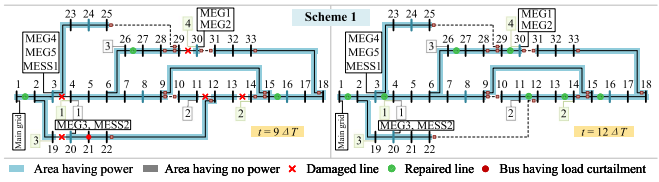

Fig. 5. Distribution network topology and load curtailment at $t' = 9$ and 12 in scheme 1.

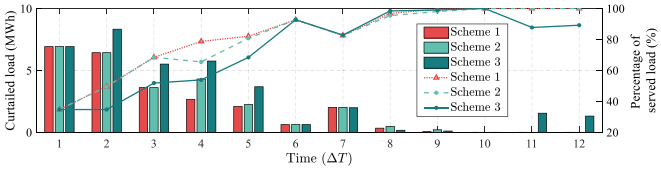

Fig. 6. Load curtailment and percentage of served load with schemes 1–3.

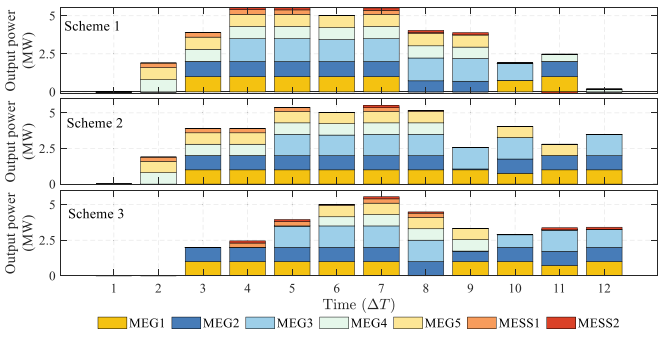

Fig. 7. Output power of MPSs with schemes 1–3.

21. At $t' = 12$, all damaged lines are repaired, and no bus has load curtailment.

Fig. 6 illustrates the load curtailment and percentage profiles of the served load at each time period with schemes 1–3. Fig. 7 illustrates the results of the output power of MPSs with schemes 1–3. As shown in Fig. 6, schemes 1–3 have the same load curtailment at $t' = 1$ as no MPS is connected with buses. In schemes 1 and 2, MEG4, MEG5, and MESS1 are connected with bus 3 at $t' = 2$, and MEG1 and MEG2 are connected with bus 30 at $t' = 3$. Moreover, the power generation of these MPSs is the same in schemes 1 and 2 at $t' = 2$ and 3. Therefore, schemes 1 and 2 have the same load curtailment at $t' = 1 - 3$. In scheme 1, due to the timely flooding mitigation by EDV1 and EDV3 on road (6,7), MEG3 and MESS2 can be connected with bus 20 at $t' = 4$ to supply power to buses 20, 22, 12, and 13. However, in scheme 2, the flooding on the routes of MEG3 and MESS2 is not mitigated in time such that MEG3 and MESS2 cannot arrive at target buses at $t' = 4$ to supply power to the distribution network. As a result, the load curtailment in scheme 1 at $t' = 4$ is significantly lower than that in scheme 2. At $t' = 5 - 12$, all MPSs are connected with the distribution network in both schemes 1 and 2, with only MESS2 being connected with different buses. Therefore, the load curtailment in schemes 1 and 2 is essentially the same after $t' = 4$. All loads are picked up after $t' = 10$ in schemes 1 and 2. The percentage of served load in scheme 3 is lower than that in schemes 1 and 2 at $t' = 2 - 5$. In particular, there is still load curtailment in the last two periods in scheme 3, even though all MPSs are connected to their target buses. As can be observed from Fig. 7, the capacity utilization rate of MPSs is maximized in the early stage of the extreme rainfall to restore the load as much as possible. In schemes 1–3, the capacity utilization rate of MPSs reaches 100% immediately after being installed at the target buses. As the damaged lines are repaired, the capacity utilization rate of MPSs decreases after $t' = 8$ in scheme 1, while the rate is still high in schemes 2 and 3.

TABLE VI
PERFORMANCE COMPARISON OF SCHEMES 1–3 UNDER DIFFERENT RAINFALL CONDITIONS

Scheme	Curtailed load (MWh)	Total travel time of MPSs (min)	Total inundation depth decreased by EDVs (m)
Extreme rainfall condition			
1	12.37	145	4.5
2	13.42	210	4.6
3	17.96	399	4.0
Heavy rainfall condition			
1	5.88	225	3.3
2	6.82	234	4.1
3	10.23	370	3.2
Moderate rainfall condition			
1	3.56	257	2.0
2	3.56	302	2.1
3	4.03	351	2.1

Table VI summarizes the statistical data of comparative performance results regarding load curtailment, total travel time of MPSs, and total inundation depth decreased by EDVs with schemes 1–3 under extreme, heavy, and moderate rainfall conditions. It is seen that under extreme (heavy) rainfall, scheme 1 can decrease the curtailed load and total travel time of MPSs by 7.8% (13.8%) and 31.0% (3.8%) compared with scheme 2, respectively, and by 31.1% (42.5%) and 63.7% (39.2%) compared with scheme 3, respectively. Besides, schemes 1 and 2 outperform scheme 3 under all rainfall conditions. Under heavy or moderate rainfall, all MPSs must be dispatched from staging locations, and some target buses of MPSs are far from staging locations, such as from node 8 to node 30. In contrast, MPSs are dispatched to buses near their staging locations under extreme rainfall. As a result, the total travel time in schemes 1 and 2 under heavy or moderate rainfall is higher than that under extreme rainfall. In addition, the load curtailment occurs centrally at $t' = 1$ and 2 under moderate rainfall. However, all MPSs in schemes 1 and 2 are only connected to the distribution network at $t' = 3$ such that the curtailed load in scheme 1 is the same as that in scheme 2 under moderate rainfall. Overall, the proposed scheme outperforms schemes 2 and 3, enabling the ETN to strengthen emergency preparedness for resilience enhancement against extreme rainfalls. In coordination with the dispatch of EDVs, MPSs can be connected to the target buses timely to cooperate with post-disaster network reconfiguration to facilitate load restoration and reduce load curtailment.

V. CONCLUSION

In this article, a robust emergency preparedness planning (EPP) scheme was proposed to coordinately pre-position diverse

Authorized licensed use limited to: Univ of Texas at Dallas. Downloaded on January 21,2024 at 03:38:14 UTC from IEEE Xplore. Restrictions apply.

mobile emergency resources (MERs) and proactively perform network reconfiguration to boost the emergency preparedness for resilience enhancement of the energy-transportation nexus (ETN) against extreme rainfalls. Specifically, a tri-level robust EPP model was developed to determine the optimal plan immunized against the worst-case realization of uncertainties in line outages and flooded roads. The key findings are summarized as follows: 1) The proposed robust EPP scheme can effectively boost the emergency preparedness of the ETN to facilitate service restoration; 2) With the coordination of mobile power sources (MPSs) and emergency drainage vehicles (EDVs), MPSs can be timely connected at the target buses to cooperate with network reconfiguration to reduce load curtailment; 3) Compared with a benchmark scheme without any emergency preparedness effort, the proposed approach can decrease the curtailed load and total travel time by 31.3% and 65.6%, respectively. The case study results have shown the effectiveness and applicability of the proposed robust EPP scheme to enhance the resilience of the ETN confronted with extreme rainfall disasters.

One limitation of the proposed scheme is that dynamic route optimization of MERs during extreme rainfalls is not considered. Moreover, the impact of uncertainties in wind power generation and electrical load on the EPP is neglected. Some of the future work for further improving the proposed scheme are: 1) Adopting real-time dynamic route optimization for the coordinated dispatch of MPSs and EDVs during the post-disaster recovery phase to decrease travel time and hasten service restoration; 2) Leveraging state-of-the-art robust optimization methods, such as data-driven distributionally robust optimization, to effectively handle uncertainties in load and renewable energy during extreme rainfalls to improve the robustness of the proposed scheme; 3) Pre-positioning MPSs, EDVs and additional MERs, such as repair crews and fuel tankers, in a coordinated manner to further enhance the resilience of the ETN under extreme rainfalls.

REFERENCES

[1] S. Fang, Z. Tian, C. Roberts, and R. Liao, "Guest editorial: Special section on toward low carbon industrial and social economy of energy-transportation Nexus," *IEEE Trans. Ind. Inform.*, vol. 18, no. 11, pp. 8146–8148, Nov. 2022.

[2] P. Zhang and S. Peeta, "A generalized modeling framework to analyze interdependencies among infrastructure systems," *Transport Res. B-Meth.*, vol. 45, no. 3, pp. 553–579, Mar. 2011.

[3] H. Gao, Y. Chen, S. Mei, S. Huang, and Y. Xu, "Resilience-oriented pre-hurricane resource allocation in distribution systems considering electric buses," *Proc. IEEE*, vol. 105, no. 7, pp. 1214–1233, Jul. 2017.

[4] B. Taheri, A. Safdarian, M. Moeini-Aghtaie, and M. Lehtonen, "Distribution system resilience enhancement via mobile emergency generators," *IEEE Trans. Power Del.*, vol. 36, no. 4, pp. 2308–2319, Aug. 2021.

[5] M. Sabbaghtorkan, R. Batta, and Q. He, "Prepositioning of assets and supplies in disaster operations management: Review and research gap identification," *Eur. J. Oper. Res.*, vol. 284, no. 1, pp. 1–19, Jul. 2020.

[6] W. Gan et al., "A tri-level planning approach to resilient expansion and hardening of coupled power distribution and transportation systems," *IEEE Trans. Power Syst.*, vol. 37, no. 2, pp. 1495–1507, Mar. 2022.

[7] X. Wang, M. Shahidehpour, C. Jiang, and Z. Li, "Resilience enhancement strategies for power distribution network coupled with urban transportation system," *IEEE Trans. Smart Grid*, vol. 10, no. 4, pp. 4068–4079, Jul. 2019.

[8] A. K. Erenoğlu, S. Sancar, İ. S. Terzi, O. Erdinç, M. Shafie-Khah, and J. P. S. Catalão, "Resiliency-driven multi-step critical load restoration strategy integrating on-call electric vehicle fleet management services," *IEEE Trans. Smart Grid*, vol. 13, no. 4, pp. 3118–3132, Jul. 2022.

[9] L. Zhang, B. Zhang, W. Tang, Y. Lu, C. Zhao, and Q. Zhang, "A coordinated restoration method of hybrid AC–DC distribution network with electric buses considering transportation system influence," *IEEE Trans. Ind. Inform.*, vol. 18, no. 11, pp. 8236–8246, Nov. 2022.

[10] M. Yan, M. Shahidehpour, A. Paaso, L. Zhang, A. Alabdulwahab, and A. Abusorrah, "Distribution system resilience in ice storms by optimal routing of mobile devices on congested roads," *IEEE Trans. Smart Grid*, vol. 12, no. 2, pp. 1314–1328, Mar. 2021.

[11] L. Zhang, S. Jiang, B. Zhang, G. Li, Z. Wang, and W. Tang, "Coordinated optimization of emergency power vehicles and distribution network reconfiguration considering the uncertain restoration capability of e-taxis," *IEEE Trans. Ind. Appl.*, vol. 58, no. 2, pp. 2707–2717, Mar./Apr. 2022.

[12] A. K. Erenoğlu and O. Erdinç, "Real-time allocation of multi-mobile resources in integrated distribution and transportation systems for resilient electrical grid," *IEEE Trans. Power Del.*, vol. 38, no. 2, pp. 1108–1119, Apr. 2023, doi: 10.1109/TPWRD.2022.3206272.

[13] S. Ghasemi and J. Moshtagh, "Distribution system restoration after extreme events considering distributed generators and static energy storage systems with mobile energy storage systems dispatch in transportation systems," *Appl. Energy*, vol. 310, Mar. 2022, Art. no. 118507.

[14] S. Lei, C. Chen, Y. Li, and Y. Hou, "Resilient disaster recovery logistics of distribution systems: Co-optimize service restoration with repair crew and mobile power source dispatch," *IEEE Trans. Smart Grid*, vol. 10, no. 6, pp. 6187–6202, Nov. 2019.

[15] C. Li et al., "Resilient outage recovery of a distribution system: Co-optimizing mobile power sources with network structure," *Protection Control Modern Power Syst.*, vol. 7, no. 3, pp. 459–471, Aug. 2022.

[16] National Petroleum Council, "Enhancing emergency preparedness for natural disasters: Government and oil & natural gas industry actions to prepare, respond, and recover, national petroleum council," 2014. Accessed: Apr. 2023. [Online]. Available: https://www.npc.org/reports/2014-Emergency_Preparedness-lr.pdf

[17] S. Lei, C. Chen, H. Zhou, and Y. Hou, "Routing and scheduling of mobile power sources for distribution system resilience enhancement," *IEEE Trans. Smart Grid*, vol. 10, no. 5, pp. 5650–5662, Sep. 2019.

[18] G. Zhang, F. Zhang, X. Zhang, Z. Wang, K. Meng, and Z. Y. Dong, "Mobile emergency generator planning in resilient distribution systems: A three-stage stochastic model with nonanticipativity constraints," *IEEE Trans. Smart Grid*, vol. 11, no. 6, pp. 4847–4859, Nov. 2020.

[19] Y. Wang, A. OulisRousis, and G. Strbac, "Resilience-driven optimal sizing and pre-positioning of mobile energy storage systems in decentralized networked microgrids," *Appl. Energy*, vol. 305, Jan. 2022, Art. no. 117921.

[20] H. Wang, Y. Liu, J. Fang, J. He, Y. Tian, and H. Zhang, "Emergency sources pre-positioning for resilient restoration of distribution network," *Energy Rep.*, vol. 6, no. 9, pp. 1283–1290, Dec. 2020.

[21] B. Li, Y. Chen, W. Wei, S. Mei, Y. Hou, and S. Shi, "Preallocation of electric buses for resilient restoration of distribution network: A data-driven robust stochastic optimization method," *IEEE Syst. J.*, vol. 16, no. 2, pp. 2753–2764, Jun. 2022.

[22] S. Lei, J. Wang, C. Chen, and Y. Hou, "Mobile emergency generator pre-positioning and real-time allocation for resilient response to natural disasters," *IEEE Trans. Smart Grid*, vol. 9, no. 3, pp. 2030–2041, May 2018.

[23] M. Yan, M. Shahidehpour, J. Lu, and X. Xu, "Coordinating electricity and transportation networks: Enhancing power grid resilience strategies against ice storms," *IEEE Electrific. Mag.*, vol. 7, no. 3, pp. 23–32, Sep. 2019.

[24] Y. Luo, S. Fang, I. Khan, T. Niu, and R. Liao, "Hierarchical robust shipboard hybrid energy storage sizing with three-layer power allocation," *IET Elect. Syst. Transp.*, vol. 13, 2023 Art. no. e12077.

[25] X. Ni, H. Huang, A. Chen, Y. Liu, and H. Xing, "Effect of heavy rainstorm and rain-induced waterlogging on traffic flow on urban road sections: Integrated experiment and simulation study," *J. Transp. Eng. Part A Syst.*, vol. 147 no. 10, Oct. 2021, Art. no. 04021057.

[26] O. Castro-Orgaz and W. H. Hager, *Shallow Water Hydraulics*. Cham, Switzerland: Springer, 2019.

[27] M. Zhang, M. Xu, Z. Wang, and C. Lai, "Assessment of the vulnerability of road networks to urban waterlogging based on a coupled hydrodynamic model," *J. Hydrol.*, vol. 603, Dec. 2021, Art. no. 127105.

Authorized licensed use limited to: Univ of Texas at Dallas. Downloaded on January 21,2024 at 03:38:14 UTC from IEEE Xplore. Restrictions apply.

[28] Q. Liu, Y. Qin, Y. Zhang, and Z. Li, "A coupled 1D–2D hydrodynamic model for flood simulation in flood detention basin," *Natural Hazards* vol. 75, pp. 1303–1325, 2015.

[29] S.-I. Nakayama, J.-I. Takayama, J. Nakai, and K. Nagao, "Semi-dynamic traffic assignment model with mode and route choices under stochastic travel times," *J. Adv. Transp.*, vol. 46, no. 3, pp. 269–281, Mar. 2012.

[30] M. Farivar and S. H. Low, "Branch flow model: Relaxations and convexfication—Part I.," *IEEE Trans. Power Syst.*, vol. 28, no. 3, pp. 2554–2564, Aug. 2013.

[31] Y. Liang, Z. Ding, T. Ding, and W. -J. Lee, "Mobility-aware charging scheduling for shared on-demand electric vehicle fleet using deep reinforcement learning," *IEEE Trans. Smart Grid*, vol. 12, no. 2, pp. 1380–1393, Mar. 2021.

[32] S. Fang, Y. Xu, S. Wen, T. Zhao, H. Wang, and L. Liu, "Data-driven robust coordination of generation and demand-side in photovoltaic integrated all-electric ship microgrids," *IEEE Trans. Power Syst.*, vol. 35, no. 3, pp. 1783–1795, May 2020.

[33] Y. Lu, Y. Liang, Z. Ding, Q. Wu, T. Ding, and W.-J. Lee, "Deep reinforcement learning-based charging pricing for autonomous mobility-on-demand system," *IEEE Trans. Smart Grid*, vol. 13, no. 2, pp. 1412–1426, Mar. 2022.

[34] Z. Ding, W. Tan, W. Lu, and W.-J. Lee, "Quality-of-service aware battery swapping navigation and pricing for autonomous mobility on demand system," *IEEE Trans. Ind. Inform.*, vol. 18, no. 11, pp. 8247–8257, Nov. 2022, doi: 10.1109/TII.2022.3172985.

[35] L. Zhao and B. Zeng, "An exact algorithm for two-stage robust optimization with mixed integer recourse problems," 2012. Accessed: May 2023. [Online]. Available: http://www.optimization-online.org/DB_FILE/2012/01/3310.pdf

[36] Y. Cao, B. Zhou, C. Y. Chung, Z. Shuai, Z. Hua, and Y. Sun, "Dynamic modelling and mutual coordination of electricity and watershed networks for spatio-temporal operational flexibility enhancement under rainy climates," *IEEE Trans. Smart Grid*, Nov. 23, 2022, early access, doi: 10.1109/TSG.2022.3223877.

[37] Z. Yang, H. Zhong, A. Bose, T. Zheng, Q. Xia, and C. Kang, "A linearized OPF model with reactive power and voltage magnitude: A pathway to improve the MW-only DC OPF," *IEEE Trans. Power Syst.*, vol. 33, no. 2, pp. 1734–1745, Mar. 2018.

[38] D. H., "Supplementary materials for case studies," 2023. Accessed: May 2023. [Online]. Available: https://doi.org/10.6084/m9.figshare.22574020.v1

Authorized licensed use limited to: Univ of Texas at Dallas. Downloaded on January 21,2024 at 03:38:14 UTC from IEEE Xplore. Restrictions apply.